Proc. Natl. Acad. Sci. USA
Vol. 89, pp. 2902–2906, April 1992
Biophysics

Spectroscopic evidence for conformational relaxation in myoglobin

[Fourier-transform infrared spectroscopy/band III (760 nm)/MbCO recombination after photodissociation]

G. ULRICH NIENHAUS, JUDITH R. MOURANT, AND HANS FRAUENFELDER†

Department of Physics, University of Illinois at Urbana–Champaign, 1110 West Green Street, Urbana, IL 61801

Contributed by Hans Frauenfelder, December 23, 1991

ABSTRACT **The time and temperature dependencies of the line area (M_0) and position (M_1) of band III at ≈760 nm have been measured with Fourier-transform infrared spectroscopy in deoxymyoglobin (Mb) and continuously photolyzed carbon monoxide myoglobin (MbCO). Below 200 K, the area of band III in the photoproduct Mb* increases with time even on time scales of hours. This behavior indicates changes in the distribution of activation enthalpy barriers for ligand rebinding under extended illumination. The band position of Mb* shifts to higher wavenumbers with increasing temperature up to 100 K owing to kinetic hole burning; the same protein coordinate that controls the position of band III also determines the rebinding barrier height. The shift ceases above 100 K, implying that more than one protein coordinate affects the height of the rebinding barrier. Above 160 K, the line position in Mb* shifts again and coalesces with the value of Mb for temperatures above 200 K. The shift is accompanied by an increase of the line area, reflecting a slowing of rebinding kinetics. Both effects are explained in the framework of the model introduced by Steinbach *et al.* [(1991) *Biochemistry* 30, 3988–4001]. Above ≈160 K, the conformational relaxation Mb* → Mb simultaneously shifts the line position of band III and increases the enthalpy barrier for ligand rebinding. Furthermore, equilibrium fluctuations lead to an averaging of the band position and the rebinding enthalpy.**

In heme proteins, photodissociation of a bound ligand leaves the protein initially in a nonequilibrium state. Above ≈160 K, this state relaxes toward the equilibrium structure, thereby creating a proteinquake (1). Starting at the heme, the proteinquake involves a sequence of conformational motions, which are reflected in subtle spectral shifts. In the present paper, we describe the motions and the corresponding spectral changes after photodissociation of carbon monoxide myoglobin (MbCO).

Mb is an oxygen storage protein with a molecular mass of ≈18 kDa and protoheme as a prosthetic group (2–4). Small ligands such as O_2 or CO bind at the heme iron. In the liganded state, the iron has spin 0 and lies close to the heme plane. In the unliganded state (Mb), the iron has spin 2 and lies ≈0.4 Å away from the mean heme plane. The globin structure differs slightly in MbCO and Mb (5–7). Immediately after photodissociation of MbCO, the globin is still in the bound-state structure. A proteinquake then releases the stored energy and leads to the Mb structure. For the present discussion, we assume that the large-scale motions are described by the scheme (1, 8, 9)

$$\mathrm{MbCO} \overset{h\nu}{\rightsquigarrow} \mathrm{Mb^{**}} \rightarrow \mathrm{Mb_2^*} \xrightarrow{\text{FIM 2}} \mathrm{Mb_1^*} \xrightarrow{\text{FIM 1}} \mathrm{Mb}. \quad [1]$$

Mb** is the state of the protein-ligand system immediately after photodissociation. At temperatures above ≈20 K, the proteinquake rapidly progresses to the state Mb_2^*, where the iron has partially moved out of the heme plane, but much of the globin is still in the bound-state structure (10–12). FIM 2 (functionally important motion) is the nonequilibrium motion that leads from Mb_2^* to Mb_1^*; it presumably involves further motion of the iron into its deoxygenated position and some motion of the proximal histidine. We associate FIM 2 with the shift of the activation enthalpy distribution observed after photodissociation at temperatures between 170 and 220 K (13, 14). The relaxation $Mb_1^* \rightarrow$ Mb (FIM 1) probably involves a shift of the F-helix to which the proximal histidine is attached. In contrast to hemoglobin, where the F-helix moves by ≈1 Å on relaxation from the ligand-bound to the deligated structure, the shift in Mb is small, so that FIM 1 has not yet been assigned to a particular experimental marker. Also, the relaxation from Mb_2^* to Mb may actually be more complex than shown in Eq. 1 and may involve more than one pathway. In view of these open questions it suffices here to discuss the spectroscopic evidence for FIM 2 in myoglobin with Mb* used for the unrelaxed and Mb used for the equilibrium structure.

As a marker for FIM 2, we use band III, a near-infrared charge-transfer transition at ≈760 nm (≈13,000 cm^{-1}) (14–21). Band III occurs only in the deligated form. Iizuka *et al.* (16) found that at 4.2 K band III was red-shifted by 14 nm in Mb* compared to Mb. At low temperatures, Mb* is metastable and band III does not relax to its deoxyMb value. At 300 K, however, Xie and Simon (22) report that band III is relaxed within 35 ps after photodissociation. Consequently, the relaxation characterized by the shift of band III, presumably FIM 2, must occur with an easily measurable rate somewhere between 4 and 300 K. We observed an apparent shift of band III starting at ≈40 K and interpreted it as evidence for FIM 2 (1). However, Friedman and collaborators (23) demonstrated that this shift did not reflect a structural relaxation but arose from kinetic hole burning (see below) (13, 24). Nevertheless, band III must shift at some temperature and reveal information about FIM 2. In the present paper, we show that the relaxation Mb* → Mb occurs above ≈160 K and is accompanied by an increase in the rebinding barrier at the heme iron (13, 14).

Methods and Materials

We exposed MbCO to continuous intense light. The competition between photolysis and rebinding led to deligated molecules, which gave rise to band III. We measured absorption spectra $\varepsilon(\nu)$ of this band at various temperatures as a function of the photolysis rate k_L and exposure time t_L. From the spectra, the area and position of band III were determined.

For the experiments, freeze-dried sperm whale Mb (Serva) was dissolved in a mixture of 75% glycerol/25% 0.4 M phosphate buffer (vol/vol), pH 6.6. The solution was deoxygenated and reduced with $Na_2S_2O_4$ to give deoxyMb. MbCO

The publication costs of this article were defrayed in part by page charge payment. This article must therefore be hereby marked "*advertisement*" in accordance with 18 U.S.C. §1734 solely to indicate this fact.

Abbreviation: FIM, functionally important motion.

†To whom reprint requests should be addressed.

was obtained by stirring for several hours under a CO atmosphere. The protein concentration of the samples was ≈15 mM. For the measurements, a few microliters of the protein solution was kept between two sapphire windows (diameter, 13 mm) separated by a 75-μm-thick Mylar washer. The windows were sandwiched inside a block of oxygen-free high-conductivity copper that was mounted on the cold finger of a closed-cycle helium refrigerator (model 22C; CTI Cryogenics, Waltham, MA). The temperature was measured with a silicon temperature sensor diode and regulated with a digital temperature controller (model DRC93C; Lake Shore Cryotronics, Westerville, OH). The MbCO sample was photolyzed with light from an argon ion laser (model 543; Omnichrome, Chino, CA). The laser was operated at 250-mW multimode output and emitted predominantly at 488 and 514 nm. The beam was split and focused with lenses on the sample from both sides. The standard photolysis rate k_L was determined as ≈20 s^{-1} at low temperatures. Lower photolysis rates were obtained by inserting calibrated neutral-density filters into the laser beam. Transmission spectra in the near infrared were collected between 12,000 and 14,000 cm^{-1} with a resolution of 8 cm^{-1} on a Fourier-transform infrared spectrometer (model Sirius 100; Mattson Instruments, Madison, WI). We used a 250-W tungsten lamp as light source, a quartz beamsplitter, and a silicon photodetector. For each spectrum, 400 mirror scans were performed during 320 s. Absorbance spectra of Mb and Mb* were calculated with MbCO background spectra taken in the dark at the same temperature. The baseline was fitted with a cubic polynomial and subtracted from the spectra. The area of band III was calculated from the absorbance $\varepsilon(\nu)$ as the zeroth moment, $M_0 = \int \varepsilon(\nu) d\nu$. The band position was computed as the first moment, $M_1 = \int \varepsilon(\nu)\nu d\nu / M_0$. The experimental results are summarized in Figs. 1 and 2.

Low-Temperature Phenomena

To untangle the phenomena displayed in Fig. 1, we first discuss the low-temperature regime between 60 and 150 K with the reaction surface shown in Fig. 3 (13, 25). In state A, the CO is bound to the heme iron. After photodissociation, the system moves to state B with the CO in the heme pocket. From there it rebinds geminately (B → A). The fraction, $N(t)$, of proteins that have not rebound a CO at time t after photodissociation is determined by a distribution of enthalpy barriers and given by

$$N(t) = \int g(H_{BA}) e^{-k(H_{BA},T)t}\, dH_{BA}. \quad [2]$$

Here $g(H_{BA})dH_{BA}$ is the probability of finding a barrier between H_{BA} and $H_{BA} + dH_{BA}$ (25, 26). The enthalpy distribution arises from the fact that the protein molecules are frozen into different conformational substates having different enthalpy barriers for rebinding. The solid curve in Fig. 4 shows $g(H_{BA})$ for MbCO (13). Above 60 K, the rebinding rate coefficient, $k(H_{BA}, T)$, is given by

$$k(H_{BA}, T) = A_{BA}(T/T_0) e^{-H_{BA}/RT}, \quad [3]$$

with the reference temperature T_0 = 100 K and the preexponential $A_{BA} = 6 \times 10^8$ s^{-1} for MbCO. Eqs. 2 and 3 together with the barrier distribution $g(H_{BA})$ describe very well the rebinding of CO to Mb after a single photolysis flash.

The Band Area $M_0(T)$. The area of band III in deoxyMb decreases continuously as the temperature increases. It is reasonable to assume that band III of a fully photolyzed MbCO sample exhibits the same temperature dependence as deoxyMb. However, only photolyzed molecules contribute to the band. Therefore, the zeroth moment depends not only explicitly on temperature but also implicitly through the temperature dependence of the photolyzed fraction, $N_B(T)$, which for a two-state model is given by

$$N_B(T) = \int \frac{k_L}{k_L + k(H_{BA}, T)}\, g(H_{BA}) dH_{BA}, \quad [4]$$

for illumination times $t_L >> 1/k_L$. Mb molecules in substates with $k(H_{BA}, T) > k_L$ rebind the ligand after each photodissociation and thus do not contribute appreciably to $N_B(T)$. Proteins with $k(H_{BA}, T) < k_L$ remain preferentially in the photolyzed state. The condition $k(H_{BA}, T) = k_L$ and Eq. 3 yield a boundary activation enthalpy

$$H_L(T) = RT \ln[A_{BA} T / k_L T_0]. \quad [5]$$

$H_L(T)$ for k_L = 20 s^{-1} and T = 100 K is indicated in Fig. 4. In a first approximation, molecules with $H_{BA} > H_L(T)$, represented by the hatched part of $g(H_{BA})$, remain in state B under steady illumination and give rise to band III. Since $g(H_{BA})$ for MbCO is well known (13, 25, 27), we can calculate $N_B(T)$ with Eq. 4 and convert it into band areas $M_0(T)$ by

$$M_0(T) = C(T) \cdot N_B(T), \quad [6]$$

where $C(T)$ accounts for the intrinsic temperature dependence of the area of band III as determined from the measurements on deoxyMb. The calculated $M_0(T)$, shown as a solid line in Fig. 1*a*, has the same general behavior as the measured $M_0(T)$ up to 150 K but disagrees quantitatively. It also fails to describe the increase of $M_0(T)$ above 150 K. Another problem emerges from Fig. 2. Eq. 4 implies that the photolyzed fraction and thus $M_0(T)$ should reach a steady state within $t_L \approx 1/k_L$, but $M_0(T)$ increases approximately

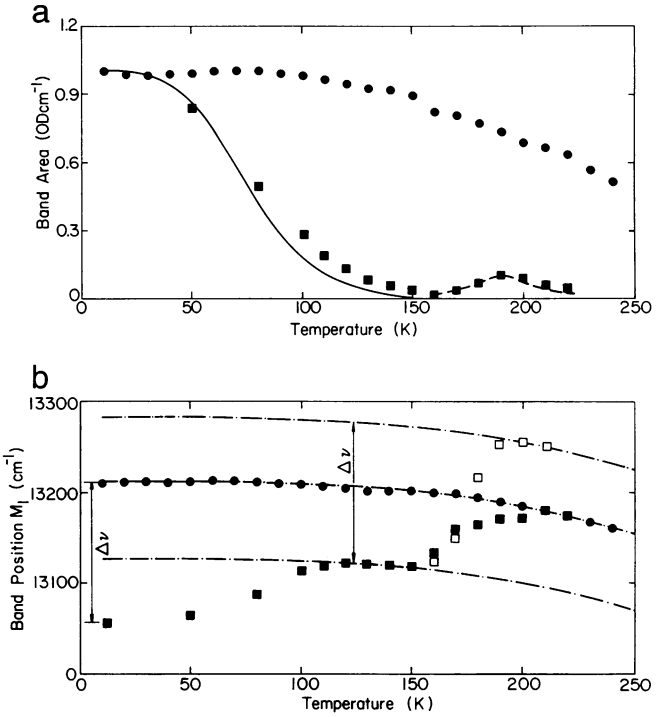

FIG. 1. Area and line position of band III in Mb as a function of temperature. ●, DeoxyMb; ■, MbCO under continuous illumination of the sample. Data were obtained from the first spectrum collected immediately after exposing the sample to the photolyzing light. (*a*) Area [zeroth moment $M_0(T)$], normalized to 1 OD·cm^{-1} at 12 K; ——, calculation with Eq. 4; - - -, calculation with Eqs. 6–10. (*b*) Band position [first moment $M_1(T)$]; □, $M_1(T)$ predicted with Eq. 11. For details, see text.

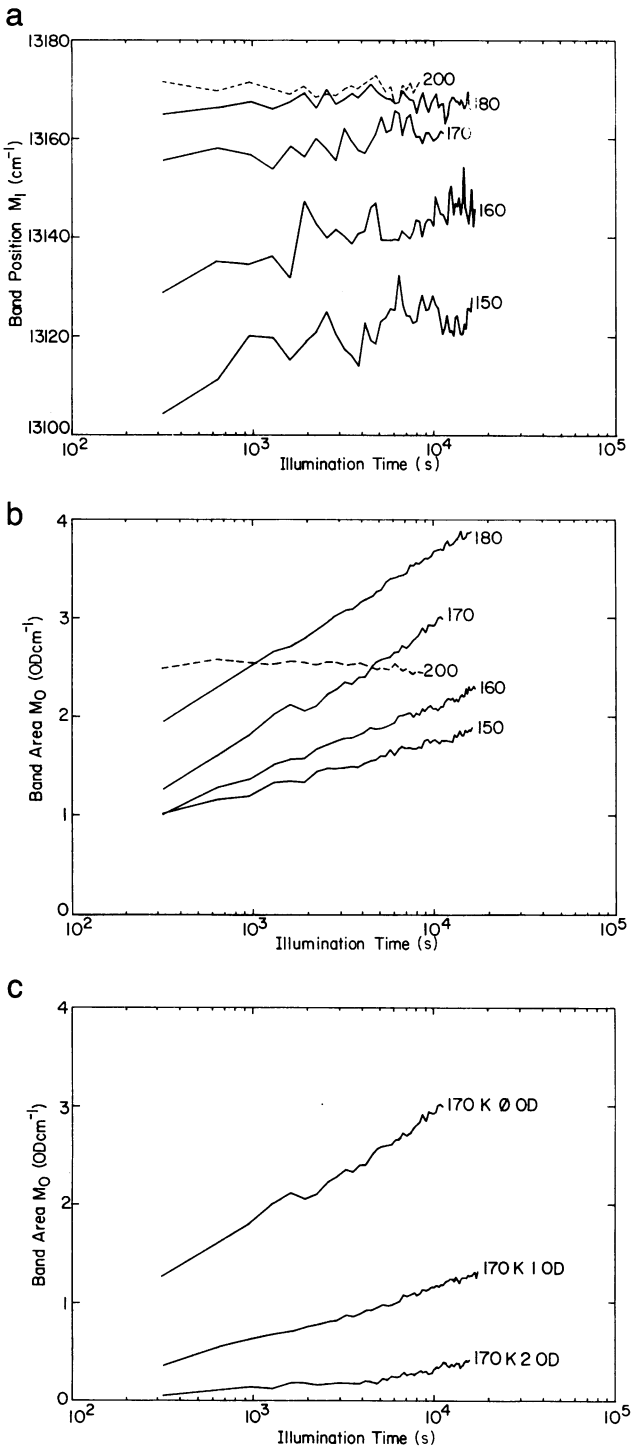

FIG. 2. Area and position of band III for various temperatures as a function of illumination time t_L. (*a*) $M_1(T)$. (*b*) $M_0(T)$. (*c*) M_0(170 K) for three photolysis beam intensities; 0 OD corresponds to photolysis rate $k_L = 20\ s^{-1}$.

logarithmically up to 180 K. This observation suggests that $g(H_{BA})$ depends on the illumination time t_L.

The observed behavior of $M_0(T)$ below 150 K can be explained by an effect discovered by Chance and collaborators (28, 29) and further studied by other groups (30–32). The rebinding of CO to Mb at low temperatures slows after prolonged illumination. Powers *et al.* (29) and Srajer *et al.* (32) explain the slowing with movements of the CO to other states in the pocket or protein matrix. Our own experiments (ref. 30; unpublished data) lead us to explain the slowing by light-induced transitions among the conformational substates. We assume that these transitions result in an effective distribution $g_L(H_{BA})$ that is shifted to higher barriers as indicated in Fig. 4. The shift depends on T, k_L, and (approximately logarithmically) the exposure time t_L. The shifted barrier distribution $g_L(H_{BA})$ explains why $M_0(T)$ is larger than expected from the low-temperature $g(H_{BA})$ between 90 and 150 K and why it depends on t_L even for $t_L >> 1/k_L$.

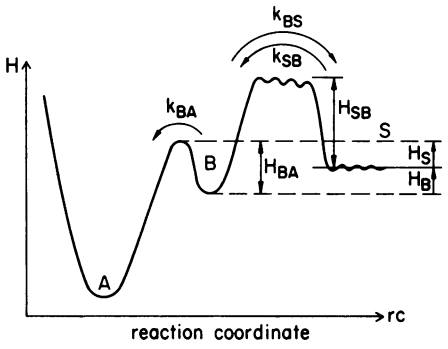

FIG. 3. Effective enthalpy H of the system Mb + CO as a function of the reaction coordinate (rc).

The Position $M_1(T)$ of Band III. Fig. 1*b* shows $M_1(T)$ of Mb and Mb*. Mb exhibits a continuous decrease of $M_1(T)$ with increasing temperature between 100 and 250 K. The behavior of Mb* is different. Between 10 and 120 K, the increase of $M_1(T)$ of Mb* is caused by kinetic hole burning (13, 23, 24). Protein molecules in different conformational substates have their band III position at slightly different wavenumbers; therefore, the band is inhomogeneously broadened. Substates with low wavenumbers have low rebinding barriers H_{BA} and thus rebind faster. Under steady illumination, only molecules with $H_{BA} > H_L(T)$ contribute to the band position $M_1(T)$. As the temperature is increased, $H_L(T)$ shifts to higher barriers; consequently, the band position moves to higher wavenumbers. In the model of Champion and coworkers (33), the enthalpy barrier H_{BA} is related to the out-of-plane distance c of the iron with respect to the heme plane. Because band III is a charge-transfer transition involving

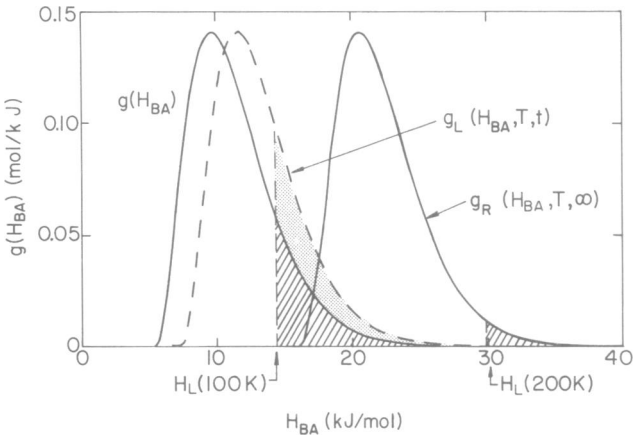

FIG. 4. Activation enthalpy distributions for ligand rebinding in MbCO. $g(H_{BA})$ denotes the barrier distribution as determined from flash photolysis experiments below 160 K; $g_L(H_{BA}, T, t)$ is the barrier distribution that is shifted because of extended illumination; $g_R(H_{BA}, T, \infty)$ gives the distribution $g(H_{BA})$ after complete relaxation Mb* → Mb. Hatched area of $g(H_{BA})$ represents the molecules that spend most of their time in the photolyzed state under steady illumination ($k_L = 20\ s^{-1}$) at 100 K. Stippled area is the fraction that adds to this population if the distribution moves up to higher enthalpies. Hatched area of $g_R(H_{BA}, T, \infty)$ shows the population that can be kept in the photolyzed state at 200 K.

both iron and porphyrin orbitals (15), it is also expected to be sensitive to c. Thus, kinetic hole burning arises from the fact that both H_{BA} and the line position ν are coupled to the same coordinate c.

$M_1(T)$ of Mb* is essentially temperature independent in the region 120–150 K. Therefore, kinetic hole burning saturates around 120 K while $H_L(T)$ still increases. This observation implies that the rebinding barrier H_{BA} is not entirely determined by the out-of-plane distance of the iron, but by at least one other coordinate, as has been suggested by Friedman *et al.* (34).

The Protein Relaxation

Major changes in protein motions occur near 180 K (1, 25, 35–37). Such changes are observable in Fig. 1. $M_0(T)$ increases again above 150 K and reaches a peak between 180 and 200 K. $M_1(T)$ also increases, and its value coincides with that of deoxyMb at and above 210 K. These features can be understood with the model of ligand binding that we introduced recently (13).

The Band Area $M_0(T)$. The increase of $M_0(T)$ above 160 K can be explained by the relaxation Mb* → Mb (13, 14). The rebinding kinetics observed in flash photolysis experiments above 160 K can be fitted by assuming that the entire $g(H_{BA})$ shifts, with each barrier increasing according to

$$H_{BA}(t, T) = H_0 + \Delta H^*[1 - e^{-[\kappa^*(T)t]^\beta}]. \quad [7]$$

Here t is the time after photodissociation. The rate coefficient $\kappa^*(T)$ does not follow an Arrhenius relation but can be described by

$$\kappa^*(T) = A^* e^{-[E^*/RT]^2}. \quad [8]$$

The relaxation parameters for MbCO in glycerol/buffer, pH 6.8, were determined from fitting the rebinding kinetics between 160 and 210 K by Eqs. 7 and 8 (13). $\Delta H^* = 11 \pm 1$ kJ/mol is the maximum shift of $g(H_{BA})$. The rate coefficient $\kappa^*(T)$ and the coefficient $\beta = 0.24 \pm 0.06$ characterize the temporal evolution of FIM 2. The parameters A^* and E^* were determined as $\log(A^*/s^{-1}) = 18 \pm 3$ and $E^* = 10 \pm 1$ kJ/mol. We denote the thermally relaxed distribution by $g_R(H_{BA}, T, t)$. The fully shifted distribution, $g_R(H_{BA}, T, \infty)$, is sketched in Fig. 4. The thermal relaxation Mb* → Mb increases the fraction of Mb molecules that have enthalpy barriers larger than $H_L(T)$. To describe the effect quantitatively, we note a simple relation. Fig. 4 implies that the photolyzed fraction under steady-state illumination $N_B^r(T, H_L)$—i.e., the area of the relaxed and shifted distribution above H_L—is the same as the unrelaxed one for $H_L^r(T) = H_L(T) - \Delta H_{BA}^r(t, T)$. Lowering of $H_L(T)$ to $H_L^r(T)$ corresponds approximately to a lowering of the temperature from T to T^r, with

$$T^r/T = H_L^r(T)/H_L(T). \quad [9]$$

We therefore have

$$N_B^r(T) \approx N_B(T^r). \quad [10]$$

Eqs. 6–10 permit us to use the experimentally measured band areas $M_0(T)$ below 150 K to predict the values above 150 K. One difficulty occurs in the evaluation of Eq. 7. The actual time $\langle t \rangle$ that must be inserted into Eq. 7 is smaller than t_L because only a fraction of the Mb molecules relax during the entire time without rebinding at least once. It will also depend on temperature. Numerical estimates indicate that for 180 K and $t_L = 320$ s, $\langle t \rangle$ is ≈50 s. The computed $M_0(T)$ (shown in Fig. 1*a* as the dashed curve) reproduces well the observed $M_0(T)$ between 160 and 220 K. A complete treatment should include the escape of ligands into the solvent. The rates of these events are very small below 200 K so that they remain undetected in single-flash photolysis kinetic traces (13, 25, 38). Steady-state experiments, however, where each molecule is photolyzed many times during the measurement, enhance the fraction of ligands moving out into the solvent and give evidence for a solvent process above ≈170 K (32). Below 220 K, the correction for this effect is small.

The Position $M_1(T)$ of Band III. Above 150 K, $M_1(T)$ increases again with temperature. We assume that the shift of $M_1(T)$ is governed by the same motion as the shift of the barrier $H_{BA}(t, T)$ and write in analogy to Eq. 7

$$M_1(t, T) = M_1(0, T) + \Delta M_1[1 - e^{-[\kappa^*(T)t]^\beta}]. \quad [11]$$

The maximal shift at pH 7, $\Delta M_1 = 156$ cm^{-1}, is obtained by comparing M_1 for deoxyMb and photolyzed MbCO at 10 K. $M_1(t, T)$ of Mb*, calculated with Eq. 11 and $\langle t \rangle = 50$ s, is shown in Fig. 1*b* as open squares. It crosses the Mb data and saturates ≈70 cm^{-1} higher after complete relaxation. This behavior can be understood. In Mb, all molecules contribute to the line. Therefore, the position is an average over the whole ensemble. In Mb*, however, only the molecules with the highest barriers in the ensemble contribute to the line under steady-state conditions. The fact that the data for the two samples coalesce above 200 K is evidence for protein fluctuations in tier 1 of the substate hierarchy of MbCO (39) at these temperatures. If a photodissociated MbCO molecule fluctuates among different substates, both H_{BA} and $M_1(T)$ will change with time. Consequently, the line position becomes a time average over all accessible substates. These protein fluctuations may already be noticeable at 180 K, where the shift of $M_1(T)$ begins to flatten out.

Two remarks must be added. The first concerns the value of ΔM_1 at temperatures around 10 K. In our earlier paper (13), we report $\Delta M_1 = 116$ cm^{-1}. Other authors give values between 131 and 239 cm^{-1} (16–19). We have found that M_1 depends on solvent composition, pH, and protein concentration. The second remark applies to substates of tier 0. Three such substates contribute to band III; they rebind and relax differently (27, 30). Therefore, the measurements described here should be repeated with samples containing the tier 0 substates with various weights. We believe, however, that the main conclusions will not be affected by this complication.

Summary and Conclusion

The experimental data presented here provide evidence for three dynamic phenomena in MbCO. Extended illumination increases the barrier for rebinding; thermal relaxation also increases this barrier, and equilibrium fluctuations average the barrier heights and open pathways for the photodissociated ligands to escape from the proteins into the solvent. The three phenomena occur at different temperatures. The light-induced transitions take place even below 10 K, thermal relaxation starts at ≈160 K, and the equilibrium fluctuations begin around 180 K.

While no detailed model for the light-induced transitions exists, the two other dynamic phenomena are explained within the framework of a hierarchy of conformational substates (1, 30) by a model that we introduced recently (13). In this model, we describe the time dependence of the thermal relaxation of the globin structure after photodissociation (14) by a stretched exponential (Eq. 7) and the temperature dependence of the rate coefficient by a Ferry law (Eq. 8). The model describes the behavior of the charge-transfer band at 760 nm at all temperatures and provides support for the existence of two crucial tiers of substates—tiers 1 and 2. Tier 1 involves large-scale motions that are responsible for opening pathways through the protein matrix. Motions in tier 2

(FIM 2) are responsible for the increase of the height of the rebinding barrier at the heme iron after photodissociation and for the shift of band III above ≈160 K.

Our spectroscopic data give little information about the structural rearrangements that occur in the relaxation processes. The x-ray structures of deoxyMb (6, 7) and ligated Mb (5, 40, 41) suggest a structural explanation for FIM 2. While only very small differences exist between the positions of most atoms in the ligated and deligated forms (42), the position of the heme iron clearly changes. Its distance from the mean heme plane is 0.03 Å in MbCO (5) and 0.35 Å in deoxyMb (6, 7). At low temperatures, motions of the protein are restricted. Therefore, it is likely that photodissociation leads to the structure Mb* where the iron has only partially moved out of the heme plane. At higher temperature, the protein becomes increasingly flexible and is able to relax into the equilibrium deoxyMb conformation.

A high-resolution x-ray structure analysis of photolyzed MbCO could support this scenario but has not yet been performed. Raman spectroscopy offers support for the hindered mobility of the heme iron in the photoproduct Mb* at low temperatures. From the shifts of Raman lines in the high-frequency region (≈1500 cm^{-1}), Rousseau and Argade (8) concluded that the heme core of Mb* is expanded compared to deoxyMb (2.027 versus 2.020 Å at 4.2 K) (8). This expansion can be explained by the increased repulsion between the occupied ($d_{x^2-y^2}$) orbital of the high-spin iron and the pyrrole nitrogen orbitals because of incomplete relaxation. Additional support comes from the increased frequency of the iron histidine stretch mode in Mb* (233 cm^{-1}) compared with deoxyMb (225 cm^{-1}) at 4.2 K (43). In Mb*, the frozen protein matrix does not allow the imidazole side chain to pull the iron out of the heme plane as much as in deoxyMb. Therefore, the optimal bond length and strength can be established, which is reflected in a large iron-histidine stretch frequency.

In our recent paper (13), we inferred the conformational relaxation Mb* → Mb from the temperature dependence of the flash photolysis rebinding and from studies of the kinetic hole burning of band III. Here we have added direct spectroscopic evidence for the conformational relaxation, as reflected in the area and position of band III above ≈160 K. While this paper focuses on the effects of protein motions on the final binding step, the entry and exit of the ligand is another crucial process in which dynamic effects are of utmost importance. Austin and collaborators (44) have recently obtained information about this step by monitoring the stretch frequency of the photolyzed CO. More work will be needed to obtain a detailed picture of the dynamic interplay between the protein and the ligand migrating into and out of the heme pocket.

We thank Jim Alben, Bob Austin, Bill Eaton, and Joel Friedman for useful remarks and Bradley T. Banko, Kelvin Chu, David Ehrenstein, Don C. Lamb, Jochen Müller, Pal Ormos, Robert Philipp, Aihua Xie, Robert D. Young, and Slobodan Zdravkovic for their collaboration and invaluable discussions. This work was supported in part by the National Science Foundation (Grant DMB87-16476), the National Institutes of Health (Grants GM 18051 and 32455), and the Office of Naval Research (Grant N00014-89-J-1300). G.U.N. thanks the Alexander von Humboldt Foundation for a Feodor Lynen Fellowship.

1. Ansari, A., Berendzen, J., Bowne, S. F., Frauenfelder, H., Iben, I. E. T., Sauke, T. B., Shyamsunder, E. & Young, R. D. (1985) *Proc. Natl. Acad. Sci. USA* **82**, 5000–5004.
2. Antonini, E. & Brunori, M. (1971) *Hemoglobin and Myoglobin in Their Reactions with Ligands* (North-Holland, Amsterdam).
3. Dickerson, R. E. & Geis, I. (1983) *Hemoglobin* (Benjamin/Cummings, Menlo Park, CA).
4. Stryer, L. (1988) *Biochemistry* (Freeman, New York).
5. Kuriyan, J., Wilz, S., Karplus, M. & Petsko, G. (1986) *J. Mol. Biol.* **192**, 133–154.
6. Phillips, S. E. V., Protein Data Bank (Brookhaven Natl. Lab., Upton, NY), accession no. 1 mbd.
7. Nienhaus, G. U. (1987) Dissertation (Univ. of Münster, Münster, F.R.G.).
8. Rousseau, D. L. & Argade, P. V. (1986) *Proc. Natl. Acad. Sci. USA* **83**, 1310–1314.
9. Rousseau, D. L. & Friedman, J. M. (1987) in *Biological Applications of Raman Spectroscopy*, ed. Spiro, T. G. (Wiley, New York), pp. 133–213.
10. Henry, E. R., Eaton, W. A. & Hochstrasser, R. M. (1986) *Proc. Natl. Acad. Sci. USA* **83**, 8982–8986.
11. Petrich, J. W., Poyart, C. & Martin, J. L. (1988) *Biochemistry* **27**, 4049–4060.
12. Petrich, J. W., Lambry, J.-C., Kuczera, K., Karplus, M., Poyart, C. & Martin, J. L. (1991) *Biochemistry* **30**, 3975–3987.
13. Steinbach, P. J., Ansari, A., Berendzen, J., Braunstein, D., Chu, K., Cowen, B. R., Ehrenstein, D., Frauenfelder, H., Johnson, J. B., Lamb, D. C., Luck, S., Mourant, J. R., Nienhaus, G. U., Ormos, P., Philipp, R., Xie, A. & Young, R. D. (1991) *Biochemistry* **30**, 3988–4001.
14. Agmon, N. & Hopfield, J. J. (1983) *J. Chem. Phys.* **79**, 2042–2053.
15. Eaton, W. A. & Hofrichter, J. (1981) *Methods Enzymol.* **76**, 175–261.
16. Iizuka, T., Yamamoto, H., Kotani, M. & Yonetani, T. (1974) *Biochim. Biophys. Acta* **371**, 1715–1729.
17. Fiamingo, F. G. & Alben, J. O. (1985) *Biochemistry* **26**, 3092–3096.
18. Srajer, V. & Champion, P. M. (1991) *Biochemistry* **30**, 7390–7402.
19. Cordone, L., Cupane, A., Leone, M. & Vitrano, E. (1990) *Biopolymers* **29**, 639–643.
20. Chavez, M. D., Courtney, S. H., Chance, M. R., Kiula, D., Nocek, J., Hoffman, B. M., Friedman, J. M. & Ondrias, M. R. (1990) *Biochemistry* **29**, 4844–4852.
21. Sassaroli, M. & Rousseau, D. L. (1987) *Biochemistry* **26**, 3092–3096.
22. Xie, X. & Simon, J. D. (1991) *Biochemistry* **30**, 3682–3692.
23. Campbell, B. F., Chance, M. R. & Friedman, J. M. (1987) *Science* **238**, 373–376.
24. Agmon, N. (1988) *Biochemistry* **27**, 3507–3511.
25. Austin, R. H., Beeson, K. W., Eisenstein, L., Frauenfelder, H. & Gunsalus, I. C. (1975) *Biochemistry* **14**, 5355–5373.
26. Frauenfelder, H., Parak, F. & Young, R. D. (1988) *Annu. Rev. Biophys. Biophys. Chem.* **17**, 451–479.
27. Steinbach, P. J., Chu, K., Frauenfelder, H., Johnson, J. B., Lamb, D. C., Nienhaus, G. U., Sauke, T. B. & Young, R. D. (1991) *Biophys. J.* **61**, 235–245.
28. Chance, B., Korszun, K., Khalid, S., Alter, C., Sorge, J. & Gabbidon, E. (1986) in *Structural Biological Applications of X-Ray Absorption, Scattering, and Diffraction*, eds. Bartunik, H. D. & Chance, B. (Academic, New York), pp. 49–71.
29. Powers, L., Chance, B., Chance, M., Campbell, B., Friedman, J., Khalid, S., Kumar, C., Naqui, A., Reddy, K. S. & Zhou, Y. (1987) *Biochemistry* **26**, 4785–4796.
30. Ansari, A., Berendzen, J., Braunstein, D., Cowen, B. R., Frauenfelder, H., Hong, M. K., Iben, I. E. T., Johnson, J. B., Ormos, P., Sauke, T. B., Scholl, R., Schulte, A., Steinbach, P. J., Vittitow, J. & Young, R. D. (1987) *Biophys. Chem.* **26**, 337–355.
31. Winkler, H., Franke, M., Trautwein, A. X. & Parak, F. (1990) *Hyperfine Interact.* **58**, 2405–2412.
32. Srajer, V., Reinisch, L. & Champion, P. M. (1991) *Biochemistry* **30**, 4886–4895.
33. Srajer, V., Reinisch, L. & Champion, P. M. (1988) *J. Am. Chem. Soc.* **110**, 6656–6669.
34. Friedman, J. M., Campbell, B. F. & Noble, R. W. (1990) *Biophys. Chem.* **37**, 43–59.
35. Doster, W., Cusack, S. & Petry, W. (1989) *Nature (London)* **337**, 754–756.
36. Nienhaus, G. U., Heinzl, J., Huenges, E. & Parak, F. (1989) *Nature (London)* **338**, 665–666.
37. Iben, I. E. T., Braunstein, D., Doster, W., Frauenfelder, H., Hong, M. K., Johnson, J. B., Luck, S., Ormos, P., Schulte, A., Steinbach, P. J., Xie, A. H. & Young, R. D. (1989) *Phys. Rev. Lett.* **62**, 1916–1919.
38. Young, R. D., Frauenfelder, H., Johnson, J. B., Lamb, D. C., Nienhaus, G. U., Philipp, R. & Scholl, R. (1991) *Chem. Phys.* **158**, 315–327.
39. Frauenfelder, H., Alberding, N. A., Ansari, A., Braunstein, D., Cowen, B. R., Hong, M. K., Iben, I. E. T., Johnson, J. B., Luck, S., Marden, M. C., Mourant, J. R., Ormos, P., Reinisch, L., Scholl, R., Schulte, A., Shyamsunder, E., Sorensen, L. B., Steinbach, P. J., Xie, A., Young, R. D. & Yue, K. T. (1990) *J. Phys. Chem.* **94**, 1024–1038.
40. Takano, T. (1977) *J. Mol. Biol.* **110**, 569–584.
41. Phillips, S. E. V. (1980) *J. Mol. Biol.* **142**, 531–554.
42. Parak, F., Heidemeier, J. & Nienhaus, G. U. (1988) *Hyperfine Interact.* **40**, 147–158.
43. Sassaroli, M., Dasgupta, S. & Rousseau, D. L. (1986) *J. Biol. Chem.* **261**, 13704–13713.
44. Hong, M. K., Shyamsunder, E., Austin, R. H., Gerstman, B. S. & Chan, S. S. (1991) *Phys. Rev. Lett.* **66**, 2673–2676.